THE ASTROPHYSICAL JOURNAL, 455:202–214, 1995 December 10

NEUTRINO CAPTURE ON HEAVY NUCLEI

GAIL C. MCLAUGHLIN AND GEORGE M. FULLER
Department of Physics, University of California San Diego, La Jolla, CA 92093-0319
Received 1995 February 20; accepted 1995 June 15

ABSTRACT

We examine the process of electron neutrino and electron antineutrino capture on nuclei with masses $A > 40$ in the context of the post–core-bounce supernova environment. We discuss the influence of final-state electron blocking, extended distributions of Gamow-Teller strength, and the Coulomb wave correction factor on neutrino and antineutrino capture rates. We study the effect of discrete state transitions and the thermal population of excited states on these rates. We estimate the strength of forbidden capture channels and discuss their importance in neutrino capture rate estimates. We find that forbidden strength can dominate the antineutrino capture rates on neutron-rich nuclei which are blocked and have no allowed transitions. Forbidden weak strength may be important in other cases of neutrino or antineutrino capture as well, depending on the excitation energy distribution of this strength. In addition, the importance of neutrino capture relative to antineutrino capture on both heavy nuclei and free nucleons is discussed. Formulae for calculating these rates in the context of the post–core-bounce supernova environment are presented. Tables of rates are provided for some key nuclei. A FORTRAN code for calculating rates is available on request.

Subject headings: elementary particles — nuclear reactions, nucleosynthesis, abundances — supernovae: general

1. INTRODUCTION

In this paper we discuss in detail the calculation of the charged current neutrino and antineutrino capture rates on heavy nuclei:

$$\nu_e + A(Z, N) \rightarrow A(Z + 1, N - 1) + e^- , \quad (1a)$$

$$\bar{\nu}_e + A(Z, N) \rightarrow A(Z - 1, N + 1) + e^+ . \quad (1b)$$

In these expressions, A, Z, and N are the nuclear mass, proton, and neutron numbers, respectively. Our study concentrates on the rates of these reactions in the region above the neutrino sphere in the post–core-bounce environment of a Type II supernova.

Neutrino capture rates on nucleons and nuclei in this environment may be important in models of nucleosynthesis from neutrino-heated supernova ejecta. In particular, neutrino capture on free nucleons sets the ratio of neutrons to protons in the late-time (time post–core-bounce $t_{pb} > 1$ s) high-entropy ($s/k > 100$) ejecta. This has been proposed as a promising r-process site (Meyer et al. 1992; Woosley et al. 1994).

The role of the processes in equations (1a) and (1b) in r-process nucleosynthesis must be small if the observed solar system abundance distribution is to be reproduced. A knowledge of the rates of these processes therefore, allows constraints to be placed on the location of the r-process region (Fuller & Meyer 1995).

Neutrino-heated supernova ejecta from earlier epochs ($t_{pb} < 1$ s), where the entropy is lower ($s/k \approx 40$), have been proposed as the site of origin of the α-process (Woosley & Hoffman 1992) and the light p-process nuclei (cf. Domogatsky & Nadyozhin 1977; Fuller & Meyer 1995; Hoffman et al. 1995). The role of the neutrino capture reactions on heavy nuclei in these nucleosynthesis processes is controversial. Neutrino capture can play no role if the neutrino-heated material outflow rate at early times is as large as one-dimensional calculations suggest (e.g., Hoffman et al. 1995). On the other hand, significant hindrance of early outflow could result in important nucleosynthesis effects from neutrino capture (Fuller & Meyer 1995). In any case, the importance of these processes for nucleosynthesis can only be judged when accurate estimates of the rates are available.

The scheme by Fuller & Meyer (1995) to utilize the processes in equations (1a) and (1b) to solve the problem of overproduction of neutron-rich nuclei and produce light p-nuclei suffers from requiring a large, and probably unrealistic, flux of neutrinos. With the rates for the processes in equations (1a) and (1b) taken from the allowed-only estimates of Fuller & Meyer (1995), material would have to loiter near a radius of ~ 100 km for a time of order ~ 0.5 s. Such conditions are not found in any one- or two-dimensional supernova model. However, if there are effects (e.g., forbidden transitions) which could increase the rates of (especially) the processes in equation (1a), the normal outflow considered in Woosley et al. (1994) might have significant and beneficial effects induced by neutrino capture on nuclei. We will discuss whether such an acceleration of neutrino capture rates might be possible.

In this paper we first present general formulae for calculating neutrino and antineutrino capture rates and give tables of rates for a few sample nuclei. A FORTRAN code is available for the calculation of the rates for these and other nuclei. The rest of this paper is devoted to examining factors which may influence the rates and discussing the relative importance of neutrino and antineutrino capture in various conditions.

Each complete rate is the sum of several transitions. In what follows we discuss the treatment of the Fermi resonance state (isobaric analog state), Gamow-Teller resonance state, general discrete state, and forbidden transitions. We also consider the effect of thermal population of excited states. We divide the rate for a single transition into two factors, one of which is a phase-space factor that contains the energy-dependent terms. The effect of electron blocking on this factor is considered along with the Coulomb wave correction factor and the effect of the distribution of the Gamow-Teller strength. The other factor, the nuclear matrix element, is estimated using the

single-particle shell model. The Gamow-Teller matrix element is calculated using the sum rule. We explain the calculation of the rates for mirror nuclei and also for $N = Z$ nuclei. We estimate the effect of forbidden transitions on the neutrino and antineutrino capture rates. Finally, we discuss the calculation of neutrino and antineutrino capture rates on free nucleons. Conclusions are given in § 11.

2. THE GENERAL PICTURE FOR NEUTRINO CAPTURE IN SUPERNOVAE

In this section we present a general formula for estimating the neutrino and antineutrino capture rates on heavy nuclei in the region above the neutrino sphere in the post–core-bounce environment of Type II supernovae. Here we adopt the general prescription for calculating neutrino and antineutrino capture rates on heavy nuclei given in Fuller & Meyer (1995). The total neutrino (antineutrino) capture rate is a sum over the rates of several transitions,

$$\lambda = \sum_i \mathscr{P}_i \sum_{ij} \lambda_{ij} \,. \tag{2a}$$

In this expression, $\mathscr{P}_i$ is the population index for the ith state of the parent nucleus,

$$\mathscr{P}_i = \frac{(2J_i + 1)e^{-E_i/kT_e}}{\mathscr{Z}} \,, \tag{2b}$$

where J_i and E_i are the spin and excitation energy of the parent nuclear state i, $\mathscr{Z}$ is the nuclear partition function of the parent, and kT_e is the local electron temperature. Of course, the plasma above the neutrino sphere is well approximated as being in thermal equilibrium, so the ions and electrons have the same temperature. The sum in equation (2a) includes all transitions, including those to the isobaric analog state and Gamow-Teller resonance state, discrete state transitions, and forbidden transitions. Following Fuller & Meyer (1995), the rate for an individual allowed transition contributing to the sum in equation (2a) can be approximated as

$$\lambda_{ij} \approx \left(\frac{R_\nu^2}{4r^2}\right) \frac{1}{(m_e c^2)^5} \frac{\ln 2}{ft_{ij}} \times \int_{E_{\rm TH}}^{\infty} G E_\nu^2 (Q_n^{ij} + E_\nu)^2 \frac{1}{\exp\,(E_\nu/kT_\nu) + 1} B_e(E_\nu) dE_\nu \,. \tag{3}$$

Here r is the radial distance from the center of the neutron star, R_ν is the radius of the neutrino sphere, T_ν is the temperature of the neutrinos or antineutrinos at the neutrino sphere, m_e is the mass of an electron, and c is the speed of light. The temperature T_ν (or $T_{\bar\nu}$) still determines the neutrino (antineutrino) distribution function even in regions well above the neutrino (antineutrino) sphere. The labels i and j refer to the transition from the ith state in the parent to the jth state in the daughter. In this expression, G is the Coulomb wave correction factor as defined in Fuller, Fowler, & Newman (1980, hereafter FFN I) and ft_{ij}, the effective ft-value, contains the nuclear matrix element. The nuclear Q-value, Q_n^{ij}, is defined as

$$Q_n^{ij} = M(Z, N)c^2 - M(Z \pm 1, N \mp 1)c^2 + E_i - E_j \,, \tag{4}$$

where the *nuclear* masses of a parent nucleus with Z protons and N neutrons and a daughter nucleus with $Z \pm 1$ protons and $N \mp 1$ neutrons are $M(Z, N)$ and $M(Z \pm 1, N \mp 1)$, respectively. The upper signs are chosen for a weak transition induced by ν_e capture, while the lower signs obtain for $\bar\nu_e$ capture. In these expressions, E_i is the excitation energy of the parent nuclear state i, and E_j is the excitation energy of the daughter nuclear state j. We take E_ν to be the neutrino or antineutrino energy as appropriate, and $E_{\rm TH}$ to be the threshold energy for the reaction. In terms of the Q-value, this threshold energy is

$$E_{\rm TH} = \begin{cases} 0 & \text{for } Q_n^{ij} \geq m_e c^2 \,, \\ -Q_n^{ij} + m_e c^2 & \text{for } Q_n^{ij} < m_e c^2 \,. \end{cases} \tag{5}$$

The final state electron blocking factor is $B_e(E_\nu)$ and is discussed in § 4. We emphasize that the expression in equation (3) is an approximation in that it assumes that the neutrino and/or antineutrino distribution functions are Fermi-Dirae. In fact these distribution functions can deviate significantly from Fermi-Dirae (see, for example, Fuller & Meyer 1995).

Writing the total capture rate in terms of the neutrino or antineutrino luminosity yields

$$\lambda_{ij} \approx \Gamma \Lambda_{ij} \,, \tag{6}$$

where Γ is the "geometrical factor" defined as

$$\Gamma \equiv \left(\frac{R_\nu^2}{4r^2}\right)\left(\frac{kT_\nu}{m_e c^2}\right)^5 \approx 12.679 \left(\frac{L_\nu}{10^{51}\ \text{ergs s}^{-1}}\right)\left(\frac{kT_\nu}{\text{MeV}}\right)\frac{1}{r_7^2} \,. \tag{7}$$

Here L_ν is the luminosity of the neutrinos or antineutrinos, and r_7 is the radius at which the capture reactions take place in units of 10^7 cm. Note that the factor Γ is proportional to the neutrino or anitneutrino flux. These fluxes decrease with increasing radius by the factor $1/r_7^2$, and increase with neutrino or antineutrino temperature.

The neutrino (antineutrino) temperature also enters into the neutrino (antineutrino) capture phase-space factor. This phase-space factor is included in Λ, the nuclear factor. If $B_e \approx 1$, then the nuclear factor for a transition between the parent state i and the daughter state j is defined as

$$\Lambda_{ij} \equiv \langle G \rangle \frac{\ln 2}{ft_{ij}} \int_{\eta_L}^{\infty} \eta_\nu^2 (\xi_n^{ij} + \eta_\nu)^2 \frac{1}{e^{\eta_\nu} + 1} d\eta_\nu \,, \tag{8a}$$

where we have defined the quantities

$$\xi_n^{ij} \equiv \frac{Q_n^{ij}}{kT_\nu} \,, \tag{8b}$$

$$m_t \equiv \frac{m_e c^2}{kT_\nu} \,, \tag{8c}$$

$$\eta_\nu \equiv \frac{E_\nu}{kT_\nu} \,, \tag{8d}$$

$$\eta_L \equiv \frac{E_{\rm TH}}{kT_\nu} \,. \tag{8e}$$

Here kT_ν represents either the neutrino or the antineutrino temperature at the neutrino sphere, as appropriate.

We estimate the rates by assuming three possible transition types for each nucleus. The transitions for neutrino capture on a nucleus with a neutron excess are shown in Figure 1*a*. Hereafter we will refer to such nuclei as neutron-rich. The $T^>$ nucleus (nucleus with the larger ground-state isospin) is the parent in this case, and the $T^<$ nucleus is the daughter. The

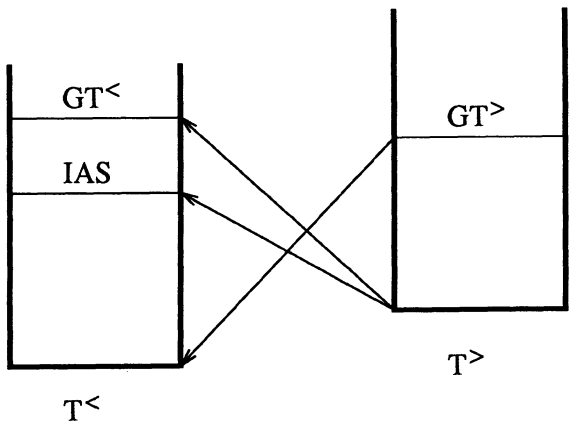

FIG. 1a

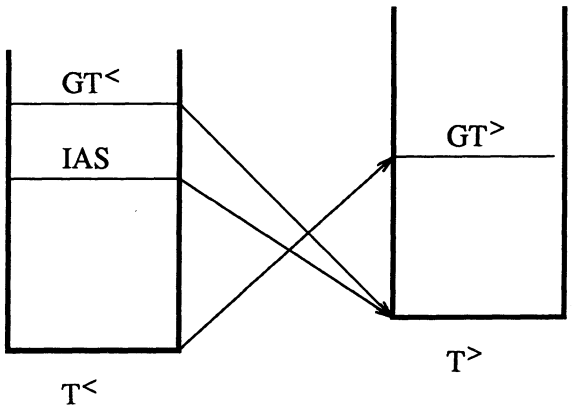

FIG. 1b

FIG. 1.—(*a*) Neutrino (antineutrino) capture transitions from a neutron-rich (proton-rich) $T^>$ parent nucleus to the $T^<$ daughter nucleus. The three transitions shown connect the parent ground state to the isobaric analog state (IAS), the parent ground state to the $GT^<$ resonance, and the thermally populated $GT^>$ resonance to the ground state of the daughter. (*b*) Antineutrino (neutrino) capture transitions from a neutron-rich (proton-rich) $T^<$ parent nucleus to the $T^>$ daughter nucleus. The three transitions included are the reverse of the processes shown in (*a*). These connect the parent ground state to the $GT^>$ resonance, the thermally populated IAS to the ground state of the daughter, and the thermally populated $GT^<$ resonance to the ground state of the daughter.

transitions shown in the figure are from the ground state of the parent to both the isobaric analog state (IAS) and the Gamow-Teller resonance in the daughter, and also from the thermally populated Gamow-Teller resonance in the parent nucleus to the ground state of the daughter. Other transitions, such as forbidden and discrete state transitions, will be discussed later. Neutrino capture on a neutron-rich nucleus can be approximated as (Fuller & Meyer 1995)

$$\lambda_{\nu_e} \approx \Gamma\left\{\Lambda^{\nu_e}_{\rm IAS} + \alpha_Q\left[\Lambda^{\nu_e}_{\rm GT<} + \Lambda^{\nu_e}_{\rm GT>}\left(\frac{\mathscr{Z}^<}{\mathscr{Z}^>}\right)\exp\left(\frac{-E_{\rm GT>}}{kT_e}\right)\right]\right\}. \quad (9a)$$

The nuclear factors for the transitions to the IAS and to the Gamow-Teller resonance are designated by $\Lambda^{\nu_e}_{\rm IAS}$ and $\Lambda^{\nu_e}_{\rm GT<}$, respectively. The nuclear factor for the transition from the thermally populated Gamow-Teller resonance in the parent to the ground state of the daughter is labeled as $\Lambda^{\nu_e}_{\rm GT>}$. The nuclear matrix element, Coulomb wave correction factor, and final-state electron blocking factor are not included in the integral part of the nuclear factor. The effect of these approximations on the rates is discussed in later sections. The factor α_Q is the Gamow-Teller quenching factor, which is approximately $\frac{1}{2}$ (cf. Fuller & Meyer 1995). Here $\mathscr{Z}^</\mathscr{Z}^>$ is the ratio of the partition functions of the daughter and parent nucleus. We define $E_{\rm GT>}$ to be the centroid energy of the Gamow-Teller resonance strength distribution in the parent. Here T_e is the electron temperature.

Figure 1*b* shows the transitions included in this estimate of the antineutrino capture rate on a neutron-rich nucleus. The transitions are the reverse of the transitions in Figure 1*a*. In this case, the nucleus may capture an antineutrino and go from the parent ground state to the Gamow-Teller resonance in the daughter. Also, the parent may make an antineutrino-induced transition from a thermally excited IAS or Gamow-Teller state to the ground state of the daughter. These transitions are included in the approximate expression for the antineutrino capture rate:

$$\lambda_{\bar{\nu}_e} \approx \Gamma\left\{\alpha_Q\left[\Lambda^{\bar{\nu}_e}_{\rm GT>} + \Lambda^{\bar{\nu}_e}_{\rm GT<}\left(\frac{\mathscr{Z}^>}{\mathscr{Z}^<}\right)\exp\left(\frac{-E_{\rm GT<}}{kT_e}\right)\right] + \Lambda^{\bar{\nu}_e}_{\rm IAS}\left(\frac{\mathscr{Z}^>}{\mathscr{Z}^<}\right)\exp\left(\frac{-E_{\rm IAS}}{kT_e}\right)\right\}. \quad (9b)$$

The situation for proton-rich nuclei is very similar. Antineutrino capture on a proton-rich nucleus is shown in Figure 1*a*. The total rate for this process can be given by the following equation:

$$\lambda_{\bar{\nu}_e} \approx \Gamma\left\{\Lambda^{\bar{\nu}_e}_{\rm IAS} + \alpha_Q\left[\Lambda^{\bar{\nu}_e}_{\rm GT<} + \Lambda^{\bar{\nu}_e}_{\rm GT>}\left(\frac{\mathscr{Z}^<}{\mathscr{Z}^>}\right)\exp\left(\frac{-E_{\rm GT>}}{kT_e}\right)\right]\right\}. \quad (9c)$$

Neutrino capture on a proton-rich nucleus is shown in Figure 1*b*. The total rate for this process can be approximated as

$$\lambda_{\nu_e} \approx \Gamma\left\{\alpha_Q\left[\Lambda^{\nu_e}_{\rm GT>} + \Lambda^{\nu_e}_{\rm GT<}\left(\frac{\mathscr{Z}^>}{\mathscr{Z}^<}\right)\exp\left(\frac{-E_{\rm GT<}}{kT_e}\right)\right] + \Lambda^{\nu_e}_{\rm IAS}\left(\frac{\mathscr{Z}^>}{\mathscr{Z}^<}\right)\exp\left(\frac{-E_{\rm IAS}}{kT_e}\right)\right\}. \quad (9d)$$

Tables of rates calculated with the above approximations for various nuclei are given in Table 1. The first column is the neutrino (antineutrino) temperature. The second and third columns show the corresponding neutrino and antineutrino capture rates. The nuclei are labeled by their nuclear charge Z and their total number of nucleons, A.

The overall magnitude of a neutrino or antineutrino capture rate is determined by the neutrino (antineutrino) temperature, luminosity, and distance from the neutron star. However, it is sometimes important to know the relative rates of neutrino and antineutrino capture on a single nucleus. This helps determine the overall neutron-to-proton ratio in some circum-

TABLE 1

CAPTURE RATES FOR VARIOUS NUCLEI AND TEMPERATURES

T (MeV) (1)	λ_ν (s^{-1}) (2)	$\lambda_{\bar\nu}$ (s^{-1}) (3)
	$^{50}_{22}$Ti	
1.....	1.5×10^{-2}	6.9×10^{-5}
2.....	5.3×10^{-1}	8.8×10^{-3}
3.....	2.1×10^{0}	4.5×10^{-2}
4.....	4.5×10^{0}	1.1×10^{-1}
5.....	7.5×10^{0}	2.0×10^{-1}
6.....	1.1×10^{1}	2.9×10^{-1}
7.....	1.4×10^{1}	4.0×10^{-1}
8.....	1.8×10^{1}	5.1×10^{-1}
9.....	2.2×10^{1}	6.1×10^{-1}
10.....	2.6×10^{1}	7.5×10^{-1}
	$^{51}_{22}$Ti	
1.....	2.3×10^{-2}	5.9×10^{-6}
2.....	6.8×10^{-1}	2.9×10^{-3}
3.....	2.6×10^{0}	2.4×10^{-2}
4.....	5.6×10^{0}	6.9×10^{-2}
5.....	9.0×10^{0}	1.3×10^{-1}
6.....	1.3×10^{1}	2.1×10^{-1}
7.....	1.7×10^{1}	2.9×10^{-1}
8.....	2.1×10^{1}	4.0×10^{-1}
9.....	2.6×10^{1}	5.3×10^{-1}
10.....	3.0×10^{1}	6.1×10^{-1}
	$^{51}_{23}$V	
1.....	1.0×10^{-2}	3.7×10^{-3}
2.....	3.8×10^{-1}	6.7×10^{-2}
3.....	1.7×10^{0}	1.9×10^{-1}
4.....	3.7×10^{0}	3.5×10^{-1}
5.....	6.1×10^{0}	5.3×10^{-1}
6.....	9.0×10^{0}	6.1×10^{-1}
7.....	1.2×10^{1}	8.5×10^{-1}
8.....	1.5×10^{1}	1.0×10^{0}
9.....	1.9×10^{1}	1.3×10^{0}
10.....	2.3×10^{1}	1.4×10^{0}
	$^{56}_{25}$Mn	
1.....	1.8×10^{-2}	1.0×10^{-3}
2.....	4.3×10^{-1}	5.1×10^{-2}
3.....	2.0×10^{0}	1.9×10^{-1}
4.....	4.4×10^{0}	4.0×10^{-1}
5.....	7.5×10^{0}	6.4×10^{-1}
6.....	1.1×10^{1}	9.3×10^{-1}
7.....	1.5×10^{1}	1.2×10^{0}
8.....	2.0×10^{1}	1.5×10^{0}
9.....	2.3×10^{1}	1.8×10^{0}
10.....	2.8×10^{1}	2.0×10^{0}
	$^{56}_{26}$Fe	
1.....	3.8×10^{-3}	2.9×10^{-3}
2.....	2.3×10^{-1}	8.8×10^{-2}
3.....	1.2×10^{0}	2.9×10^{-1}
4.....	2.9×10^{0}	5.6×10^{-1}
5.....	5.2×10^{0}	8.8×10^{-1}
6.....	8.3×10^{0}	1.2×10^{0}
7.....	1.1×10^{1}	1.6×10^{0}
8.....	1.4×10^{1}	1.9×10^{0}
9.....	1.7×10^{1}	2.2×10^{0}
10.....	2.1×10^{1}	2.6×10^{0}
	$^{56}_{27}$Co	
1.....	4.2×10^{-3}	1.5×10^{-2}
2.....	1.1×10^{-1}	5.3×10^{-1}
3.....	6.4×10^{-1}	9.6×10^{-1}
4.....	1.7×10^{0}	1.4×10^{0}
5.....	3.2×10^{0}	1.8×10^{0}
6.....	5.1×10^{0}	2.4×10^{0}
7.....	7.1×10^{0}	2.7×10^{0}
8.....	9.8×10^{0}	3.2×10^{0}
9.....	1.2×10^{1}	3.7×10^{0}
10.....	1.4×10^{1}	6.7×10^{0}
	$^{60}_{27}$Co	
1.....	6.5×10^{0}	2.6×10^{-1}
2.....	8.3×10^{0}	6.1×10^{-1}
3.....	1.1×10^{1}	1.0×10^{0}
4.....	1.5×10^{1}	1.4×10^{0}
5.....	2.0×10^{1}	1.7×10^{0}
6.....	2.5×10^{1}	2.2×10^{0}
7.....	3.2×10^{1}	2.4×10^{0}
8.....	3.8×10^{1}	2.9×10^{0}
9.....	4.4×10^{1}	3.2×10^{0}
10.....	5.0×10^{1}	3.7×10^{0}
	$^{60}_{28}$Ni	
1.....	2.5×10^{-3}	6.7×10^{-2}
2.....	2.0×10^{-1}	4.0×10^{-1}
3.....	1.1×10^{0}	8.5×10^{-1}
4.....	2.9×10^{0}	1.3×10^{0}
5.....	5.3×10^{0}	1.8×10^{0}
6.....	8.3×10^{0}	2.4×10^{0}
7.....	1.1×10^{1}	2.9×10^{0}
8.....	1.5×10^{1}	3.5×10^{0}
9.....	1.9×10^{1}	3.7×10^{0}
10.....	2.3×10^{1}	4.5×10^{0}
	$^{60}_{29}$Cu	
1.....	1.0×10^{-3}	9.1×10^{-2}
2.....	9.0×10^{-2}	4.8×10^{-1}
3.....	6.2×10^{-1}	1.0×10^{0}
4.....	1.7×10^{0}	1.5×10^{0}
5.....	3.5×10^{0}	2.2×10^{0}
6.....	5.5×10^{0}	2.6×10^{0}
7.....	8.3×10^{0}	3.2×10^{0}
8.....	1.1×10^{1}	3.7×10^{0}
9.....	1.4×10^{1}	4.5×10^{0}
10.....	1.6×10^{1}	5.1×10^{0}
	$^{64}_{29}$Cu	
1.....	3.5×10^{-3}	3.2×10^{-3}
2.....	2.7×10^{-1}	8.0×10^{-2}
3.....	1.4×10^{0}	2.6×10^{-1}
4.....	3.5×10^{0}	4.8×10^{-1}
5.....	6.4×10^{0}	7.5×10^{-1}
6.....	9.8×10^{0}	1.0×10^{0}
7.....	1.4×10^{1}	1.3×10^{0}
8.....	1.7×10^{1}	1.6×10^{0}
9.....	2.2×10^{1}	1.9×10^{0}
10.....	2.6×10^{1}	2.2×10^{0}
	$^{64}_{30}$Zn	
1.....	1.7×10^{-3}	8.5×10^{-3}
2.....	1.6×10^{-1}	1.5×10^{-2}
3.....	9.0×10^{-1}	4.3×10^{-1}
4.....	2.5×10^{0}	7.7×10^{-1}
5.....	4.7×10^{0}	1.2×10^{0}
6.....	7.4×10^{0}	1.6×10^{0}
7.....	1.1×10^{1}	2.0×10^{0}
8.....	1.4×10^{1}	2.4×10^{0}
9.....	1.7×10^{1}	2.9×10^{0}
10.....	2.0×10^{1}	3.2×10^{0}
	$^{92}_{42}$Mo	
1.....	3.7×10^{-4}	1.7×10^{-2}
2.....	1.1×10^{-1}	1.0×10^{-1}
3.....	8.3×10^{-1}	2.2×10^{-1}
4.....	2.4×10^{0}	3.5×10^{-1}
5.....	4.9×10^{0}	4.8×10^{-1}
6.....	8.3×10^{0}	6.1×10^{-1}
7.....	1.1×10^{1}	7.2×10^{-1}
8.....	1.6×10^{1}	8.5×10^{-1}
9.....	2.0×10^{1}	1.0×10^{0}
10.....	2.4×10^{1}	1.1×10^{0}
	$^{96}_{44}$Tc	
1.....	2.6×10^{-4}	4.0×10^{-2}
2.....	9.0×10^{-2}	2.2×10^{-1}
3.....	7.5×10^{-1}	4.5×10^{-1}
4.....	2.4×10^{0}	6.9×10^{-1}
5.....	5.0×10^{0}	9.6×10^{-1}
6.....	8.3×10^{0}	1.2×10^{0}
7.....	1.2×10^{1}	1.5×10^{0}
8.....	1.7×10^{1}	1.7×10^{0}
9.....	2.1×10^{1}	2.0×10^{0}
10.....	2.6×10^{1}	2.2×10^{0}

NOTE.—Neutrino and antineutrino capture rates are shown for several nuclei at various temperatures. Col. (1) indicates the neutrino or antineutrino temperature as appropriate in MeV. Cols. (2) and (3) give the corresponding capture rates. The neutrino and antineutrino luminosities are each taken to be equal to 3.5×10^{51} ergs s^{-1}. The rates in these tables were calculated assuming a radius of 100 km.

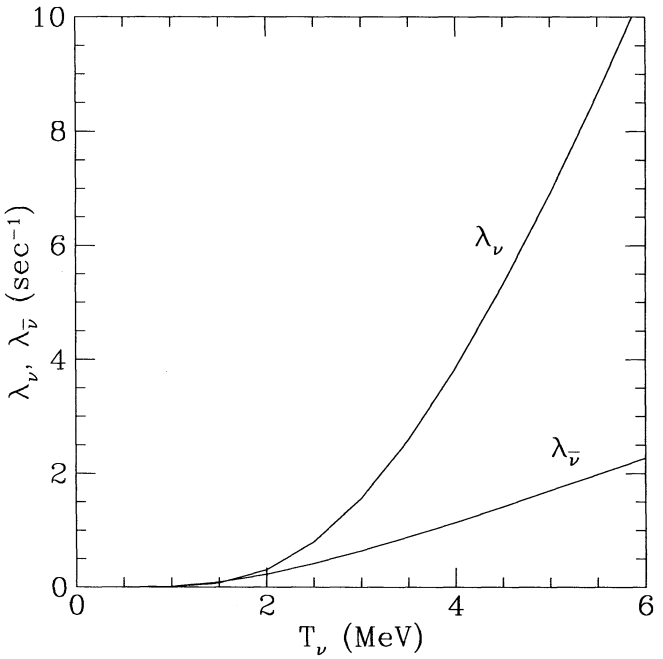

FIG. 2.—Neutrino and antineutrino capture rates (λ_{ν_e} and $\lambda_{\bar\nu_e}$, respectively) on ^{56}Fe, plotted against neutrino temperature, T_{ν_e} (MeV). The ratio of antineutrino to neutrino temperature is taken here to be constant at 1.23.

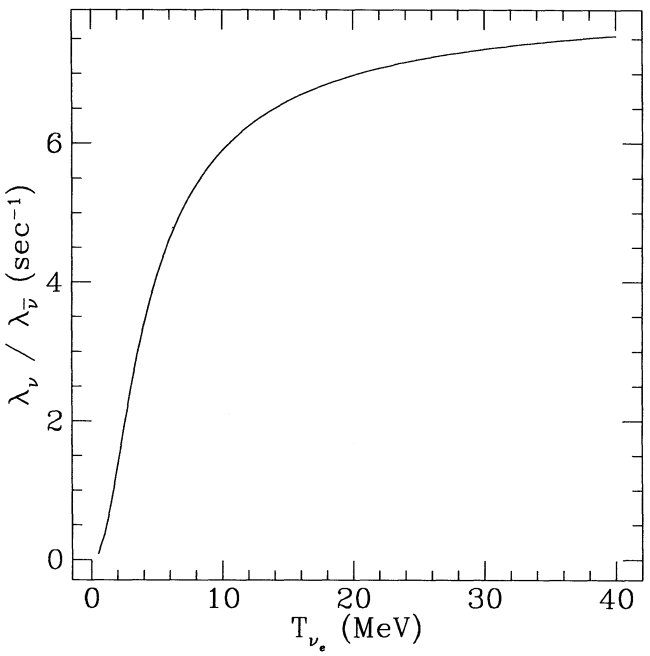

FIG. 3.—Ratio of the neutrino capture rate to the antineutrino capture rate as a function of neutrino temperature. As in Fig. 2, the ratio of neutrino to antineutrino temperature is taken to be constant at 1.23.

stances (e.g., Fuller & Meyer 1995). This comparison depends on differences in the neutrino and antineutrino luminosities and temperatures, and the structure of the nuclei involved in the transition.

Figure 2 plots the neutrino and antineutrino rates on the nucleus ^{56}Fe. There is more strength in the nuclear matrix element for neutrino capture in this case, but at low temperatures the antineutrino capture is similar to the neutrino capture rate. For a neutrino to capture into the Fermi resonance state in the daughter ^{56}Co, it needs an energy of at least 7.6 MeV. In contrast, for an antineutrino to capture into the Gamow-Teller resonance in ^{56}Mn, it needs an energy of 7.0 MeV. This difference in threshold energy causes the neutrino capture rate to be comparable to the antineutrino capture rate at low energies. In Figure 3 the ratio of neutrino to antineutrino capture rates is plotted against neutrino temperature for the nucleus ^{56}Fe. The ratio of T_{ν_e} to $T_{\bar\nu_e}$ is taken here as constant at 1.23. However, $\lambda_{\nu_e}/\lambda_{\bar\nu_e}$ is not constant until relatively high neutrino energy, 30 or 40 MeV. At such high neutrino energies, the threshold is less important and the neutrino capture rate is larger than the antineutrino capture rate. Neutrino and antineutrino capture rates are sensitive to nuclear properties through nuclear matrix elements and nuclear Q-values.

3. NUCLEAR MATRIX ELEMENTS

In this section the matrix elements for Fermi and Gamow-Teller transitions are discussed. We consider both the distribution of strength of the matrix elements and the total strength in each type of transition.

For neutrino capture on neutron-rich nuclei, the transitions from the ground state of the parent proceed to the IAS and Gamow-Teller resonances in the daughter, as shown in Figure 1*a*. The Fermi operator is the isospin raising and lowering operator, which commutes with the strong interaction parts of the nuclear Hamiltonian. Therefore, the distribution of Fermi strength appears as one state in the daughter nucleus and thus is taken here to be a delta function. The Fermi matrix element is

$$|M_F|^2 = |N - Z| . \tag{10}$$

The total strength of the Gamow-Teller operator is governed by the sum rule,

$$S_{\beta^-} - S_{\beta^+} = 3(N - Z) , \tag{11}$$

where S_{β^+} is the sum of the Gamow-Teller matrix elements for $\bar\nu_e$ capture, and S_{β^-} is the sum of Gamow-Teller matrix elements for ν_e capture. The S_{β^+} matrix element is calculated as in Fuller, Fowler, & Newman (1982, hereafter FFN II) from the single-particle model. When the nucleus is neutron-rich, $Z < N + 1$, it is clear that S_{β^-} exceeds S_{β^+}. When the nucleus is very neutron-rich, the Gamow-Teller transitions in the $\bar\nu_e$ capture direction can be blocked, in which case

$$S_{\beta^+} = 0 . \tag{12}$$

Such blocking of S_{β^+} usually obtains for nuclei of interest in the production of the r-process and p-process elements. However, $Y_e = 1/(n/p + 1)$, the electron fraction, is more readily influenced by neutrino and antineutrino capture on iron-peak elements than by captures on heavier r-process or p-process elements in, for example, the scheme for p-process production in Fuller & Meyer (1995). Iron-peak elements have significant S_{β^+} strength, so we must write

$$S_{\beta^-} = S_{\beta^+} + 3(N - Z) . \tag{13}$$

Including the additional term, S_{β^+}, in the matrix element results in an increased neutrino capture rate. Table 2 shows the neutrino capture rates for various iron-peak nuclei, along with the percentage contribution to the matrix element from S_{β^+}. As

TABLE 2

EFFECT OF S_{β^+} ON NEUTRINO CAPTURE RATES

Nucleus (1)	$3\|N-Z\|$ (2)	$3\|N-Z\|+S_{\beta^+}$ (3)	λ_{GT} (4)	% from S_{β^+} (5)
^{56}Cr.....	24	32.57	4.97	26
^{56}Mn.....	18	28.39	3.50	36
^{56}Fe.....	12	24.00	2.39	50
^{56}Co	6	19.71	1.56	70

NOTE.—Shown is the effect of S_{β^+} on the rate of neutrino capture to the Gamow-Teller resonance. Col. (5) shows the percentage contribution of the term S_{β^+} to the Gamow-Teller rate.

is shown in the table, the effect of S_{β^+} on the total neutrino capture rate increases for smaller $(N-Z)$.

Another important consideration in calculating the Gamow-Teller transition is the distribution of strength in the daughter nucleus. The Gamow-Teller resonance, unlike the isobaric analog state, does not appear as a single state. The strength must be summed over transitions to all possible Gamow-Teller daughter states. Each such transition can be taken to have strength S^{ij}, so that the total strength from the state i of the parent nucleus is

$$S^i_{\rm tot} = \sum_j S^{ij} \,. \tag{14}$$

We approximate the sum as an integral over an energy-dependent strength function normalized by the total Gamow-Teller strength,

$$S^i_{\rm tot} = |M_{\rm GT}|^2 \int_{E_{\rm gs}}^{\infty} \mathscr{S}(E) dE \,. \tag{15}$$

Here $|M_{\rm GT}|^2$ is the total Gamow-Teller matrix element, either S_{β^+} or S_{β^-}, depending on the transition. For example, in the case of neutrino capture on a neutron-rich nucleus, we take $|M_{\rm GT}|^2 = S_{\beta^-}$.

In order to investigate the dependence of the neutrino or antineutrino capture rates on the assumed form of the strength function, we employ a Gaussian distribution for Gamow-Teller strength,

$$\mathscr{S}(E) = \exp\left[\frac{-(E-E_c)^2}{k^2 T_{\nu_e}^2 w^2}\right] \Big/ \int_{E_{\rm gs}}^{\infty} \exp\left[\frac{-(E-E_c)^2}{k^2 T_{\nu_e}^2 w^2}\right] dE \,, \tag{16}$$

where $E_{\rm gs}$ is the energy of the ground state of the daughter nucleus, and E_c is the energy of the centroid of the resonance, which is calculated as in FFN II. Here T_{ν_e} is the temperature of the neutrino distribution, and w is the width of the distribution. The result of varying w for the process of antineutrino capture on ^{56}Mn is shown in Table 3. As the distribution flattens, the Gamow-Teller rate begins to increase. This is due to the additional strength that can be accessed by lower energy neutrinos. However, once appreciable strength extends all the way to the ground state, further flattening pushes more strength to higher energies than it does to lower energies. This leads to a decrease in the rate. The maximum rate that can be achieved by adjusting w is shown in Table 4. This type of adjustment changes the rate by at most 150% for these typical iron-peak nuclei. The maximum change that could be obtained would occur in nuclei with E_c far above $E_{\rm gs}$.

The matrix element for the transition from the Gamow-Teller resonance in the parent to the daughter ground state is simply S_{β^+} for the daughter nucleus, calculated as in FFN II. For antineutrino capture on a neutron-rich nucleus, shown in Figure 1*b*, most of the rate comes from capture to the Gamow-Teller resonance. The matrix element for this transition is S_{β^+} for the parent nucleus. The other two processes used in the calculations here, thermal excitations of the Fermi and Gamow-Teller resonances in the parent to the ground state of the daughter, are calculated in the usual way. The Fermi matrix element is $(N-Z+2)$ and the Gamow-Teller matrix element is

$$S_{\beta^-} = S_{\beta^+} + 3(N-Z+2) \,. \tag{17}$$

The analogous cases for proton-rich nuclei are calculated similarly. For antineutrino capture, depicted in Figure 1*a*, the Fermi matrix element is $|N-Z|$ and the Gamow-Teller matrix element is

$$S_{\beta^+} = S_{\beta^-} + 3(Z-N) \,. \tag{18}$$

Here S_{β^-} is calculated using the single-particle shell model as in FFN II. It is the same as the calculation of S_{β^+} in the neutron-rich case, except that in this case the neutrons take the

TABLE 3

NEUTRINO CAPTURE ON ^{56}Mn

w (1)	λ_ν (s^{-1}) (2)	w (1)	λ_ν (s^{-1}) (2)
0.....	3.50	5.....	4.89
0.5.....	3.53	10.....	3.50
1.....	3.80	20.....	2.1

NOTE.—Effect of different assumed distributions of Gamow-Teller strength on the ^{56}Mn neutrino capture rate is shown. The results presented here assume a Gaussian distribution for Gamow-Teller strength. Col. (1) shows the width of the Gaussian distribution, w, and col. (2) shows the total neutrino capture rate. The neutrino temperature was taken as 4.3 MeV, the luminosity as 3.5×10^{51} ergs s^{-1}, and the distance from the neutron star was assumed to be 10^7 cm.

TABLE 4

NEUTRINO CAPTURE RATE

Nucleus (1)	λ_ν, Delta Function (2)	Maximum λ_ν (3)	w (4)
^{56}Cr.....	4.97	6.22	2.3
^{56}Mn.....	3.50	5.22	3.3
^{56}Fe.....	2.39	2.68	1.5
^{56}Co	1.56	2.08	2.4

NOTE.—Some effects of varying Gamow-Teller strength distributions on neutrino capture rates are illustrated. (1) gives the target nucleus, and col. (2) gives the rate for that nucleus assuming a delta-function Gamow-Teller strength distribution. The results presented in col. (3) assume a Gaussian distribution of Gamow-Teller strength in the computation of the neutrino capture rates. This column gives the maximum rate which can be obtained by adjusting the width w, while col. (4) gives the corresponding width. The neutrino temperature was taken as 4.3 MeV, the luminosity as 3.5×10^{51} ergs s^{-1}, and the distance from the neutron star was assumed to be 10^7 cm.

place of protons and vice versa. The matrix element for the transition from the Gamow-Teller resonance in the parent to the ground state of the daughter is given by S_{β^-} for the daughter nucleus.

In the case of neutrino capture on a proton-rich nucleus, shown in Figure 1*b*, the Gamow-Teller matrix element is S_{β^-} for the parent. The rate contributions of the transitions from the thermally populated Fermi and Gamow-Teller resonances in the parent to the ground state of the daughter are given by the Fermi and Gamow-Teller matrix elements of the daughter nucleus.

4. PHASE-SPACE INTEGRAL

The phase-space integral in the nuclear factor accounts for the energy dependence in the rate. The phase-space integral for an individual allowed transition is taken here to be

$$P^{ij} = \frac{1}{(kT_\nu)^5} \int_{E_{\rm TH}}^{\infty} G(E_\nu) E_\nu^2 (Q_n^{ij} + E_\nu)^2 \times B_e(E_\nu) \frac{1}{\exp(E_\nu/kT_\nu) + 1} dE_\nu . \quad (19a)$$

The phase-space factor for a resonance transition can be thought of as a sum over individual transitions,

$$P^i = \sum_j P_{ij} S^{ij} . \quad (19b)$$

Again, we approximate the sum as an integral,

$$P^i = \frac{1}{(kT_\nu)^5} \int_{E_{gs}}^{\infty} \mathscr{S}(E) dE \int_{E_{\rm TH}}^{\infty} G(E_\nu) E_\nu^2 (Q_n^i + E_\nu)^2 \times B_e(E_\nu) \frac{1}{\exp(E_\nu/kT_\nu) + 1} E_\nu . \quad (20a)$$

The outside integral is over energies in the daughter nucleus, and E_{gs} is the daughter ground-state energy relative to the ground state of the parent nucleus, so that

$$Q_n^i = -E . \quad (20b)$$

The additional energy-dependent factors included here are the final-state electron blocking factor, the Coulomb wave correction factor, and the strength function for the matrix element.

The final-state electron blocking factor is represented by the term

$$B_e(E_\nu) = 1 - \frac{1}{\exp[(E_\nu + Q_n^{ij} - \mu_e)/kT_e] + 1} . \quad (21)$$

Here kT_e is the temperature of the electrons and μ_e is the total electron chemical potential (including $m_e c^2$). The effect of this term in the phase-space integral is to reduce the rate. However, for typical electron temperatures in the post–core-bounce supernova,

$$kT_e < 1 \text{ MeV} , \quad (22)$$

the effect is minimal. The effect of the blocking factor on the neutrino capture rate induced by the Gamow-Teller transition is shown in Table 5. The blocking effect is more pronounced for higher electron temperature. However, even at an electron temperature of 5 MeV, the rate is reduced by only about 90%.

The Coulomb wave correction factor accounts for the attraction (repulsion) of the electron (positron) in the final state. It corrects for the approximation assumed here, that the electron or positron is in a plane-wave state. The Coulomb wave correction factor is defined as in FFN I,

$$G(\pm Z, E_e) \equiv \frac{p_e}{E_e} F(\pm Z, E_e) . \quad (23a)$$

Here p_e is the final-state electron or positron momentum, and E_e is the electron or positron final-state energy. The Fermi factor is $F(\pm Z, E_e)$, where the upper signs are for neutrino capture and the lower signs are for antineutrino capture. The Fermi factor is defined as

$$F(\pm Z, E_e) \approx 2(1+s)(2pR)^{2(s-1)} e^{\pi y} \left| \frac{\Gamma(s+iy)}{\Gamma(2s+1)} \right|^2 , \quad (23b)$$

with

$$s = [1 - (\alpha Z)^2]^{1/2} \quad (23c)$$

and

$$y = \pm \frac{\alpha Z E_e}{p_e} . \quad (23d)$$

The fine-structure constant is α.

TABLE 5

FINAL-STATE ELECTRON BLOCKING EFFECTS ON NEUTRINO CAPTURE RATES

Nucleus (1)	No blocking (2)	$T_e = 0.5$ MeV, $\mu_e = 0$ MeV (3)	$T_e = 5$ MeV, $\mu_e = 0$ MeV (4)	$T_e = 0.5$ MeV, $\mu_e = 1$ MeV (5)
^{56}Mn	3.50	3.50	3.26	3.49
^{208}Pb.....	4.85	4.84	4.46	4.83
^{92}Mo	1.55	1.55	1.43	1.54

NOTE.—Effects of final-state electron phase-space blocking on the rate of neutrino capture are shown. For illustrative purposes we consider here only Gamow-Teller contributions to neutrino capture rates. Col. (2) gives the rates for the indicated nuclei assuming no final-state electron blocking. Cols. (3)–(5) give the rates including electron blocking for a Fermi-Dirac electron distribution with the indicated electron temperature (T_e) and chemical potential (μ_e).

The Coulomb wave correction factor depends on the electron energy and nuclear charge. This is illustrated by Tables 6 and 7. In Table 6 the temperature of the incoming neutrino is varied for neutrino capture on ^{60}Ni. This effectively varies the distribution of the outgoing electron energy. The transition rate to the Gamow-Teller resonance, calculated with and without the Coulomb wave correction factor, is shown in the table. The last column shows the average Coulomb correction factor for the corresponding neutrino temperature. Table 7 shows the average Coulomb wave correction factor for neutrino capture on various nuclei. It can be seen that this factor, ≈ 1.5, exhibits relatively little variation for the various nuclei and conditions explored in the tables. For relativistic final-state leptons, $G_{\bar{\nu}_e} \approx G_{\nu_e} \exp(-2\pi\alpha Z)$ (FFN I). For the purposes of nucleosynthesis in supernovae, nuclei which have the largest neutrino capture rates have $Z \sim 30$, so $G_{\bar{\nu}_e} \sim 0.25 G_{\nu_e} \sim 0.4$.

5. THERMAL EXCITATION OF BACK RESONANCES

Thermal excitation of a resonance in the parent nucleus usually leads to only a small contribution to the total rate. We will call such a thermally populated state a "back resonance." For example, in Figure 1*a* the back resonance is the Gamow-Teller resonance state in the parent nucleus. This resonance

TABLE 6

COULOMB CORRECTION FOR $^{60}_{28}Ni_{32}$

T_ν (MeV) (1)	λ_{GT} (s^{-1}) (2)	λ_{GT} with G (s^{-1}) (3)	$\langle G \rangle$ (4)
1.....	1.32×10^{-3}	2.13×10^{-3}	1.61
2.....	6.21×10^{-2}	9.75×10^{-2}	1.57
3.....	0.490	0.757	1.54
4.....	1.42	2.16	1.53
5.....	2.76	4.16	1.51
6.....	4.39	6.58	1.50
7.....	6.23	9.27	1.49
8.....	8.23	12.2	1.48
9.....	10.3	15.2	1.47
10.....	12.5	18.2	1.46

NOTE.—Effect of the Coulomb correction factor on the rate of neutrino capture on $^{60}_{28}Ni_{32}$ is shown. Col (1) shows the neutrino temperature in MeV. Cols. (2) and (3) show the rate with and without the Coulomb correction factor. Col. (4) shows the average Coulomb correction factor for that temperature. Here we consider only the Gamow-Teller contribution to the overall neutrino capture rate.

state transition goes directly to the ground state of the daughter, and the contribution to the rate in this case comes from the last term in equation (9a). In a transition like this, there is usually no energy threshold for neutrino capture. Of course, the absence of an energy threshold implies an enhanced phase-space factor for a given neutrino energy spectrum. In general, however, this enhancement of the phase-space factor does not compensate for the effect of the small Boltzmann factor arising in the thermal population of the back-resonance state. Note that the rate contribution from the thermally populated back-resonance state is proportional to the ratio of the parent and daughter nucleus partition functions. We approximate the ratio of the partition functions in this case to be unity for the electron temperatures which are relevant for the nucleosynthesis region in the post–core bounce supernova environment (Fuller & Meyer 1995). With this assumption, it is the Boltzmann factor in the population index which limits the contribution of the back-resonance transition to the rates. When the electron temperature is around a few hundred keV, the back-resonance state must be relatively low-lying in parent excitation energy in order to be significantly populated.

TABLE 7

COULOMB CORRECTION

Nucleus (1)	λ_{GT} (2)	λ_{GT} with G (3)	$\langle G \rangle$ (4)
$^{60}_{28}Ni_{32}$.....	1.66	2.53	1.52
$^{64}_{30}Zn_{34}$	1.39	2.14	1.53
$^{59}_{28}Ni_{31}$.....	1.36	2.07	1.52
$^{58}_{28}Ni_{30}$.....	1.08	1.65	1.53
$^{96}_{44}Ru_{52}$	1.22	1.91	1.56
$^{92}_{42}Mo_{50}$.....	1.17	1.83	1.56
$^{78}_{36}Kr_{42}$	0.91	1.42	1.57
$^{56}_{24}Cr_{32}$.....	3.31	4.87	1.47
$^{56}_{25}Mn_{31}$.....	2.33	3.45	1.48
$^{56}_{26}Fe_{30}$.....	1.59	2.37	1.49
$^{56}_{27}Co_{29}$	1.04	1.57	1.51

NOTE.—Table is similar to Table 6, except that here we show the Gamow-Teller contribution to the neutrino capture rates for various nuclei without (col. [2]) and with (col. [3]) Coulomb phase-space corrections. The neutrino temperature is assumed here to be 4.5 MeV. The average Coulomb correction factor for each nucleus is shown in col. (4).

An example of such a low-lying back resonance can be found in ^{60}Co. Antineutrino capture on ^{60}Ni is dominated by a transition to the Gamow-Teller resonace in ^{60}Co. Using the formula given by FFN II for the energy of the Gamow-Teller resonance, we would predict the resonance to lie near the ground state of ^{60}Co. In this case, a candidate for a Gamow-Teller resonance state may be found in the Table of Isotopes (Browne et al. 1978). All experimentally determined nuclear level information utilized in this paper is taken from this reference. The spin and parity of the ground state of ^{60}Ni are represented by 0^+, and the lowest-lying candidate for the Gamow-Teller resonance in ^{60}Co is the 1^+ state at an energy of 0.7388 MeV. Since this state is at such low energy, it has a significant thermal population which is very sensitive to the electron temperature.

Table 8 shows the neutrino and antineutrino capture rates at a given electron temperature for ^{60}Co. The antineutrino capture is not sensitive to the electron temperature, since the IAS and Gamow-Teller resonance in ^{60}Co are at much higher energies than the ground state. However, the neutrino capture rate is very sensitive to temperature because of the importance of the thermal population of the back resonance. Figure 4 shows the total neutrino capture rate on ^{60}Co and also the portion of the total rate which comes from the back resonance. At high electron temperatures, the back resonance contributes a significant portion of the rate, while at low temperatures it is much less important.

How often are thermally populated back resonances important in neutrino and antineutrino capture rates? They are only important when the back resonance in the parent nucleus occurs very close to the ground state. In neutron-rich nuclei, this situation is rare for neutrino capture reactions and occurs, if at all, in antineutrino capture. When the Gamow-Teller spin-flip transition from the daughter to the parent results in the occupation of the same orbital that is occupied by the parent in the ground-state configuration, the resonance will be low-lying. These cases will have behaviour similar to the above example. In proton-rich nuclei the situation is exactly the

TABLE 8

THERMAL EXCITATION OF BACK RESONANCE: CAPTURE RATES FOR ^{60}Co

T_e (MeV) (1)	λ_{ν_e} (s^{-1}) (2)	$\lambda_{\bar{\nu}_e}$ (s^{-1}) (3)	T_e (MeV) (1)	λ_{ν_e} (s^{-1}) (2)	$\lambda_{\bar{\nu}_e}$ (s^{-1}) (3)
0.1.....	4.98	1.52	0.6.....	8.55	1.52
0.2.....	5.28	1.52	0.7.....	9.23	1.52
0.3.....	6.02	1.52	0.8.....	9.90	1.52
0.4.....	6.92	1.52	0.9.....	10.4	1.52
0.5.....	7.80	1.52	1.0.....	10.9	1.52

NOTE.—Neutrino and antineutrino capture rates on ^{60}Co are shown at various values of the electron temperature T_e, given in MeV. Thermal excitation of the back resonance causes the neutrino rate to vary with electon temperature. The neutrino and antineutrino temperatures were taken to be 4 MeV each in this example.

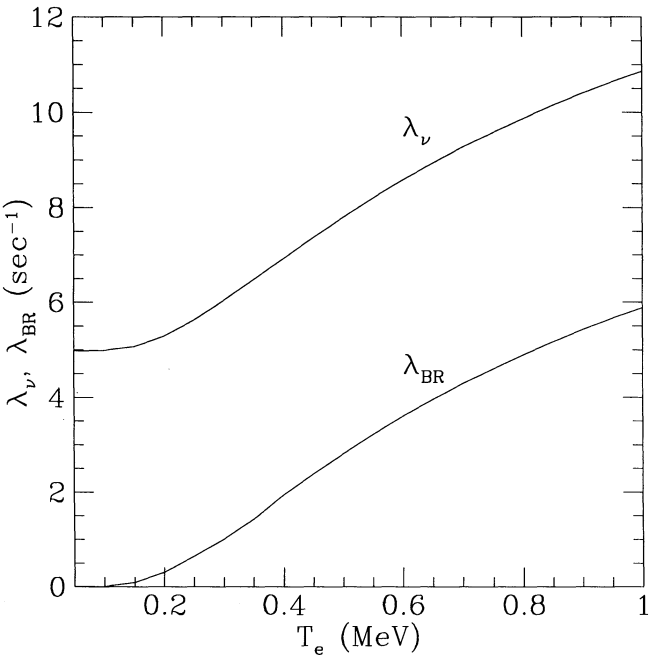

FIG. 4.—Plot of the neutrino capture rate for ^{60}Co against electron temperature. The upper curve is the total capture rate, and the lower curve is the contribution to the rate from the back resonance. As the electron temperature increases, the thermal population of the back resonance increases, resulting in a greater contribution of the back-resonance transition to the total rate.

opposite. There are a few neutrino capture cases on proton-rich parent nuclei for which this effect is important.

6. MIRROR AND $N = Z$ NUCLEI

This section is devoted to the calculation of neutrino and antineutrino capture rates of mirror and $N = Z$ nuclei.

6.1. *Mirror Nuclei*

Figure 5 shows the transitions for mirror nuclei. Neutrino capture in mirror nuclei is calculated using almost the same method as for other nuclei. In the case where $N = Z + 1$, the neutrino capture induces transitions to Fermi and Gamow-Teller states in the $N = Z - 1$ nucleus. However, since these nuclei are mirrors, the Fermi resonance is the ground state of the $N = Z - 1$ daughter nucleus. For these cases, we put the Gamow-Teller resonance the usual distance in excitation energy above the Fermi resonance (cf. Fuller & Meyer 1995). Antineutrino capture on the $N = Z + 1$ nucleus results in the usual transition to the Gamow-Teller resonance.

For the mirror nucleus, $N = Z - 1$, antineutrino capture induces transitions to the IAS and Gamow-Teller resonance in the $N = Z + 1$ nucleus. The IAS of the $N = Z - 1$ nucleus is simply the ground state of the $N = Z + 1$ nucleus. Neutrino capture on the ground state of the $N = Z - 1$ nucleus proceeds to the Gamow-Teller resonance, as shown in Figure 5.

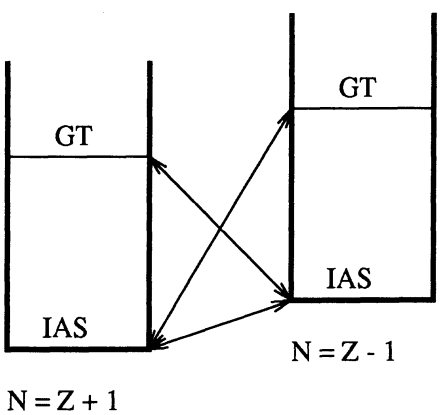

FIG. 5.—Neutrino (antineutrino) transitions between mirror nuclei. The IAS of the ground state of one of the pair of mirror nuclei is the ground state of the other member of the pair. Three transitions are included for each of the mirror nuclei. These are the transition between ground states, the transition from the ground state of the parent to the Gamow-Teller resonance in the daughter, and the transition from the thermally populated Gamow-Teller resonance in the parent to the ground state of the daughter.

6.2. *$N = Z$ Nuclei*

Capture on $Z = N$ nuclei is shown in Figure 6. The prescription for calculating rates for these nuclei is slightly different than for other elements. There is no Fermi strength, since $|N - Z| = 0$. For the same reason,

$$S_{\beta^+} = S_{\beta^-} , \tag{24}$$

so the strength for Gamow-Teller capture is the same in both directions and is estimated here using the FFN prescription. The $Z = N$ nucleus contains four resonance states, a Fermi and Gamow-Teller resonance for the $N = Z - 2$ and $N = Z + 2$ nuclei. We included transitions resulting from thermal population of these states in the calculation of the rates. However, as is true for most back resonances, these rarely have a significant effect in the total rate.

7. DISCRETE-STATE TRANSITIONS

In our calculations we have assumed the effects of discrete-state transitions on the overall neutrino and antineutrino capture rates to be negligible. In this section we will examine the validity of this assumption.

The total neutrino or antineutrino capture rate is given by equation (2a). In principle, this sum should include all tran-

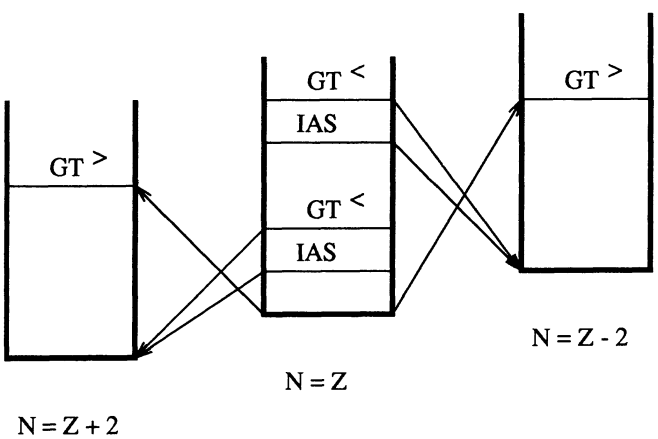

FIG. 6.—Captures to and from $N = Z$ nuclei are shown. The $N = Z$ nucleus neutrino captures to a Gamow-Teller resonance in the daughter, $N = Z - 2$. It contains Fermi and Gamow-Teller resonances which may be thermally populated, allowing transitions to the ground state of the daughter. The $N = Z$ nucleus can also antineutrino capture to a Gamow-Teller resonance in the antineutrino-capture daughter, $N = Z + 2$. The $N = Z$ parent nucleus contains an additional Fermi and Gamow-Teller resonance which may be thermally populated and allow a transition to the ground state of the antineutrino-capture daughter.

sitions to discrete states. A typical *ft*-value for a Gamow-Teller resonance transition is about $\log_{10}(ft) \approx 2.5$ for the cases considered in this paper. Hereafter, all logarithms denoted by "log" are understood to be to base 10. Experimentally measured discrete-state transitions in beta decay have log (*ft*) values far larger than that for a typical Gamow-Teller resonance transition. Therefore, in order for these transitions to be important, either there must be many of them or they must have a very large energetic advantage. For a discrete-state transition to have a rate contribution which is comparable to that from a Gamow-Teller resonance transition, we would have to have

$$N \frac{P_i}{\langle ft \rangle_i} = \frac{P_{\rm res}}{\langle ft \rangle_{\rm res}}, \tag{25}$$

where N is the number of discrete-state transitions, P_i is the typical phase-space integral and $\langle ft \rangle_i$ is the typical *ft*-value of one of these discrete transitions. Here $P_{\rm res}$ is the phase-space integral for the Gamow-Teller resonance transition, and $\langle ft \rangle_{\rm res}$ is the corresponding *ft*-value for this transition. If we approximate all discrete-state transitions as no-threshold cases, and all Gamow-Teller resonance transitions as threshold cases, then we can arrive at an approximate expression for the relationship of the *ft*-values, the *Q*-values, and the number of discrete-state transitions required for these to be competitive with a single Gamow-Teller resonance transition. This expression represents an upper limit, since not all discrete-state transitions will be no-threshold cases, and some Gamow-Teller resonance transitions will not be threshold cases. With these caveats we can transform equation (25) into such an upper limit:

$$\begin{aligned} \log \langle ft \rangle_i - \log N \approx\ & 0.43(\xi_{\rm res} + m_e c^2/kT_\nu) \\ & - \log (1 + 0.5\xi_{\rm res} + 0.083) \\ & + \log (0.97 + 0.47\xi_i + 0.075\xi_i^2) \\ & + \log \langle ft \rangle_{\rm res}, \end{aligned} \tag{26}$$

where ξ_i and $\xi_{\rm res}$ are typical *Q*-values scaled by neutrino temperature (see eq. [8b]) for discrete-state and resonance-state transitions, respectively.

Since the discrete-state transitions have, on average, large *ft*-values, it would require the contribution of many of these transitions in order for them to have significant influence on the total neutrino or antineutrino capture rate. Clearly, if only a small number of discrete-state transitions contribute, then these would need to have a small average *ft*-value to be significant.

For example, ^{90}Kr can capture a neutrino to become ^{90}Rb. In the laboratory, ^{90}Kr beta-decays 63% of the time to the 1.6882 MeV state in ^{90}Rb with a log (*ft*)-value of 4.3. The *Q*-value for this reaction is 3.2 MeV. Suppose we compare neutrino capture rate contributions of discrete-state transitions to those from the Gamow-Teller resonance transition in this case, assuming a neutrino temperature of 4 MeV. For this example, the Gamow-Teller resonance log (*ft*)-value is 1.9, and the *Q*-value for this resonance transition is -10.7 MeV. According to equation (26), we must have $\log N \approx 1.8$ in order for discrete-state transitions to be comparable to the Gamow-Teller resonance transition in their contribution to the total rate. We conclude that, for this example, there must be ~ 50 discrete-state transitions to make a rate contribution comparable to that of the resonance transition. In general, these transitions will not be important in the total neutrino capture rate. However, some cases with many discrete- state transitions and low average *ft*-values may be important.

8. RELATIVE NEUTRINO AND ANTINEUTRINO CAPTURE RATES

In this section we present a brief discussion of the relative importance of neutrino and antineutrino capture rates. For a given nucleus, the differences in these rates are determined by several factors. One factor is the ratio of the ν_e luminosity to the $\bar{\nu}_e$ luminosity. The appropriate luminosity appears in the geometrical factor Γ, so that each rate is proportional to the neutrino or antineutrino luminosity. In the post–core-bounce supernova environment at late times the luminosity of the antineutrinos is larger than that of the neutrinos. This favors the antineutrino capture rate. This is also true of the neutrino and antineutrino temperatures. At early times after the core bounce, the neutrino and antineutrino temperatures are nearly equal. At later times they begin to diverge, and the antineutrino temperature becomes larger. The geometrical factor is also proportional to the neutrino (antineutrino) temperature. However, the total rate has a more complicated temperature dependence, since the temperature appears also in the phase-space factor. It is the ratios of the *Q*-value and the threshold energy to the appropriate neutrino temperature which enter the expression for the phase-space factor. A higher neutrino or antineutrino temperature changes the phase-space integral as well as the geometrical factor. Since in the post–core-bounce supernova environment the antineutrinos have a higher temperature and luminosity than the neutrinos, this tends to increase the antineutrino capture rate relative to the neutrino capture rate. However, for the relevant neutrino and antineutrino temperatures, the Coulomb wave correction tends to increase the neutrino capture rates over the antineutrino capture rates, partially compensating for the effect of the difference between T_ν and $T_{\bar{\nu}}$.

The nuclear excitation energies of the resonance states influence the neutrino and antineutrino capture rates by determining the *Q*-values and the threshold energies. The Fermi and GT$^<$ resonance excitation energies measured relative to the parent ground state are independent of nuclear masses, but the GT$^>$ resonance excitation energy is not. The threshold energy and *Q*-value are dependent on the charge and the number of nucleons in the nucleus, the nuclear configuration, and the nuclear mass difference. For example, for an antineutrino capturing on a neutron-rich nucleus, the Gamow-Teller resonance will be at a higher *Q*-value if the daughter nucleus has a larger ground-state mass than the parent nucleus. The excitation energies of the resonances influence the rates through the phase-space factor.

The last factor which influences the differences in the rates is the matrix element. The Fermi and GT$^<$ matrix elements depend on the isospin of the nucleus, but both Gamow-Teller matrix elements depend on nuclear structure details. The exception to this is the case of blocked nuclei, which lack a GT$^>$ resonance. Neutron-rich nuclei have larger matrix elements for neutrino capture than for antineutrino capture. Proton-rich nuclei have larger matrix elements for antineutrino capture. The $Z = N$ nuclei have equal matrix elements.

Neutrino and antineutrino capture rates for some nuclei in the $A = 56$ chain are shown in Table 9. From the consideration

TABLE 9

CAPTURE RATES FOR $A = 56$

Nucleus (1)	λ_{ν_e} (s^{-1}) (2)	$\lambda_{\bar{\nu}_e}$ (s^{-1}) (3)
$^{56}_{25}Mn_{31}$	5.83	0.72
$^{56}_{26}Fe_{30}$	3.56	0.98
$^{56}_{27}Co_{29}$	2.82	2.06

NOTE.—Neutrino and antineutrino capture rates on various $A = 56$ nuclei are shown. The nucleus for which the neutrino and antineutrino rates are closest to equal is $^{56}_{24}Co_{29}$. In this example the neutrino temperature is taken to be 4.3 MeV and the antineutrino temperature is taken to be 5.3 MeV. The luminosities are taken to be $L = 3.5 \times 10^{51}$ ergs s^{-1} each for neutrinos and antineutrinos.

of matrix elements alone, it would appear that the neutrino and antineutrino capture rates should be equal for nuclei with $Z = N$. If the antineutrinos are more energetic, and have a greater luminosity, then the nuclei with equal rates will lie slightly on the higher N side of the $Z = N$ nucleus. The most tightly bound nucleus in an isobaric chain is on the neutron-rich side of $Z = N$. Because of mass differences, the nucleus which best approximates nearly equal neutrino and antineutrino capture rates tends to be close to but on the neutron-rich side of the most tightly bound nucleus in an isobaric chain.

9. FIRST-FORBIDDEN TRANSITIONS

The weak interaction Hamiltonian contains the term

$$H_{\rm weak} \propto \exp\,[i(q_\nu - p_e)\cdot x]\,, \tag{27}$$

where $q_\nu = (E_\nu, \boldsymbol{q}_\nu)$ is the 4-momentum of the incoming neutrino or antineutrino, p_e is the 4-momentum of the outgoing electron or positron, and x is the spacetime coordinate, $x = (t, \boldsymbol{x})$. Here the time component in the argument of the exponential gives the usual energy-conserving delta function in Fermi's golden rule. It is customary to expand the spatial argument of the exponential to give

$$H_{\rm weak} \propto 1 + i(\boldsymbol{q}_\nu - \boldsymbol{p}_e)\cdot \boldsymbol{x}\,. \tag{28}$$

The first term in this expression corresponds to the allowed approximation for Fermi or Gamow-Teller transitions, while the second term corresponds to the first-forbidden term. In Table 1 we have included only Fermi and Gamow-Teller transitions.

When the forbidden term is incorporated into the rate calculation it leads to the selection rules for changes in total angular momentum, ΔJ, and parity, $\Delta\pi$, of $\Delta J = 0, \pm 1, \pm 2$, no $0 \rightarrow 0$, $\Delta\pi$ = yes. In terms of the single-particle shell model, this means that forbidden operators can induce transitions between shells, for example, *fp* shell → *gd* shell.

The first-forbidden term in the weak Hamiltonian results in a first-forbidden term in the phase-space factor of order $(pR)^{(2l)}$. Here p is the momentum transfer in the neutrino capture process, R is the radius of the nucleus, and l is the order of forbiddenness. In first-forbidden transitions $l = 1$. For a typical nucleus of interest here, the radius is $R \sim 5$ fermis. If the momentum transfer, which we approximate as the Q-value, in a first-forbidden transition is about 5 MeV, then $(pR)^{2l} \sim 0.016$. If the Q-value is 10 MeV, then $(pR)^{2l} \sim 0.06$. This is an estimate of the factor by which the forbidden rate would be reduced relative to the allowed rate, all other considerations (e.g., matrix element, Q-value) being equal.

For a first-forbidden rate,

$$\lambda_{\rm for} \propto \Gamma P\,|\,M_{\rm for}\,|^2\,. \tag{29}$$

The geometrical factor is the same as in the allowed transitions. However, the phase-space factor and matrix element change. For the phase-space factor P, we use the first-forbidden unique ($\Delta J = \pm 2$) case. At high temperature, the first-forbidden unique transition is faster than the other first-forbidden transitions (Zyranova 1963; Fuller 1982). The first-forbidden unique phase-space factor is defined by Zyranova (1963) as

$$P_{\rm unique} = \frac{1}{(kT_\nu)^5}\frac{1}{12}\frac{R^2}{(\hbar c)^2}\int_{E_{\rm TH}}^{\infty} E_\nu^2(E_\nu - Q)^2(E_\nu^2 - (E_\nu - Q)^2) f_\nu\, dE_\nu\,. \tag{30}$$

We will use this phase-space factor as another way to estimate the magnitude of the first-forbidden rates. By using this method, all of the momentum dependence is absorbed in the phase-space factor. The rates are sensitive to neutrino or antineutrino temperature through the Fermi-Dirac distribution function for the neutrinos or antineutrinos, f_ν. As this temperature increases, the rates becomes larger.

The matrix element for the forbidden transitions ($l = 1$) is much larger than the matrix element for the allowed transitions ($l = 0$), since there are many more possible forbidden transitions. In order to estimate the dependence of the rates of the forbidden transitions on underlying nuclear parameters, we will include all of the first-forbidden strength with the first-forbidden unique phase-space factor. This may lead to an overestimate of the first-forbidden strength. On the other hand, detailed studies of first-forbidden *nonunique* phase-space factors have not been performed for the conditions we consider. We regard the treatment of forbidden phase-space factors as an uncertainty which should be investigated in future work.

Yet another uncertainty involving forbidden neutrino capture transitions is the distribution and location of forbidden strength. There is some *p-n* reaction evidence for "collected" first-forbidden strength (Bertsch & Esbensen 1987) at about 10 MeV in excitation energy above the position of the Gamow-Teller resonance in ^{90}Zr. This feature is seen in the *p-n* reaction data (Gaarde et al. 1981) at larger laboratory scattering angles than those for $l = 0$ transitions. The excitation energy splitting between the centroid of this $l = 1$ strength and the GT resonance, 10 MeV, is about the energy of one shell model oscillator level for this nucleus.

There are several possibilities for the placement of the first-forbidden strength. Three of these possibilities include collection at one oscillator level above the GT resonance, collection at a lower energy, or a wide and essentially flat distribution of forbidden strength with excitation energy. The centroid of the distribution of the forbidden strength is very important in calculating the magnitude of the forbidden rates. The spread of the distribution has less of an effect on the rates than does the location of the centroid, as discussed in § 3. Therefore, in estimating the first-forbidden rates we will assume a delta-function

distribution. The higher the first-forbidden strength lies, the smaller the rate will be. This is due to the increasing energy threshold and the decreasing Q-value in the phase-space factor.

As an example, we consider neutrino capture on ^{90}Zr. The Gamow-Teller resonance is calculated to lie at an excitation energy of $E_{GT<} \approx 9.5$ MeV in the daughter, ^{90}Nb. If we place the first-forbidden strength at one oscillator level above the Gamow-Teller strength, then it will be at $E_{for} \approx 19$ MeV in excitation energy. The corresponding phase-space factors are $P_{unique} \approx 0.05$ and $P_{GT} \approx 5.3$. In calculating these phase-space factors, we have assumed a neutrino temperature of 4 MeV. The forbidden phase-space factor is much smaller than the allowed phase-space factor, seeming to imply that the forbidden rate should be smaller. However, the matrix elements must also be considered. There are 110 $l = 1$ transitions in a zero-order single-particle shell model for ^{90}Zr. If we assume that the matrix element for each transition is approximately 1, then $|M_{for}|^2 \approx 110$. The Gamow-Teller matrix element in the same model is $|M_{GT}|^2 \approx 30$. In this case, the ratio of the rates is

$$\frac{\lambda_{for}}{\lambda_{GT}} \sim 0.04 . \tag{31}$$

In order for the first-forbidden transitions to be important, the matrix element must compensate for the small phase-space factor. However, if we place the collected forbidden strength at the *same* energy as the Gamow-Teller resonance, then we find $P_{unique} \approx 0.4$. In this case, the forbidden rates are no longer negligible:

$$\frac{\lambda_{for}}{\lambda_{GT}} \sim 0.3 . \tag{32}$$

Forbidden strength is also important in antineutrino capture on the nucleus ^{90}Zr, e.g., ^{90}Zr($\bar{\nu}_e$, e^+)^{90}Y. Because the nucleus is blocked in this case, there is no allowed strength in the antineutrino capture direction. However, this does not mean that the antineutrino capture rate is negligible. From the Seeger & Howard (1975) single-particle energies we estimate the forbidden strength to lie at 5 MeV above the ground state of ^{90}Y. This estimate was obtained by employing a typical single-particle orbital energy difference. The forbidden phase-space factor in this case is estimated to be $P_{unique} \approx 1.1$, assuming the antineutrino temperature is 5 MeV. This number is larger than it would be in the neutrino capture direction, owing to the difference in temperature between the neutrinos and antineutrinos. There are about 60 $l = 1$ transitions from the zero-order single-particle shell model ground state of ^{90}Zr to ^{90}Y, so the ratio of the neutrino to the antineutrino capture rates for ^{90}Zr is roughly

$$\frac{\lambda_\nu}{\lambda_{\bar{\nu}}} \sim \left(\frac{4}{5}\right)\left(\frac{5.3}{1.1}\right)\left(\frac{30}{60}\right)\left(\frac{1.5}{0.4}\right) \sim 7 . \tag{33}$$

Here λ_ν includes only the Gamow-Teller contribution to the total rate. Therefore, owing to the Fermi contribution, the ratio $\lambda_\nu/\lambda_{\bar{\nu}}$ will be larger than indicated in equation (33). The first term in equation (33) is the ratio of temperatures in the geometrical factor, the second term is the ratio of phase-space factors, the third term is the ratio of matrix elements, and the last term is the ratio of the Coulomb wave correction factors. We approximate the forbidden Coulomb correction factors to be the same as the allowed Coulomb correction factors. In this example, we have assumed equal neutrino and antineutrino luminosities. This example shows the forbidden antineutrino capture rate to be smaller than the allowed neutrino capture rate. However, it is clear from this example that forbidden transitions are not always negligible in computations of neutrino capture rates.

From the above discussion, we conclude that first-forbidden transitions are especially important in calculating neutrino and antineutrino capture rates when the Gamow-Teller strength is blocked, or if the Gamow-Teller strength is small. In addition, forbidden transitions are important if the center of their strength distribution is low-lying in daughter nucleus excitation energy resulting in a low Q-value. Consider the case of a neutron-rich nucleus near $N = Z$, where the Gamow-Teller strength in the antineutrino capture direction is blocked, the neutrino capture Gamow-Teller strength is not large, and the antineutrino capture daughter is at lower mass than the parent. In this case, the first-forbidden antineutrino capture rate contribution may begin to compete with the allowed neutrino capture rate contribution. We note that the forbidden phase-space factor is temperature dependent and increases with temperature more rapidly than the allowed phase-space factor. This implies that as the neutrino and antineutrino temperature increase, the forbidden rates become a more important part of the total capture rates. In our tables of neutrino and antineutrino capture rates we have neglected the forbidden rates. However, in an environment where nuclei have a longer exposure to neutrino fluxes or where the neutrino energies are higher, the forbidden capture contributions should be included in any rate estimate.

We wish to emphasize that the treatment of forbidden channels is the most uncertain aspect of any estimate of neutrino and antineutrino capture rates. We have shown above that the location of this forbidden strength in daughter nucleus excitation energy is a crucial determinant of the importance of forbidden transitions. If this strength is collected near or above the Gamow-Teller resonance position, then forbidden contributions are small and will not change, for example, conclusions about the efficacy of nuclear neutrino capture made by Fuller & Meyer (1995).

However, if the forbidden strength is relatively low-lying in daughter nucleus excitation energy, then reliable computation of neutrino or antineutrino capture rates becomes problematic. These issues should be investigated with detailed numerical shell model calculations. For example, the scenario for p-process production by Fuller & Meyer (1995) would be more plausible, and would require far less hydrodynamic fine-tuning, if forbidden contributions could increase the average neutrino capture rate by a factor ~ 10.

10. FREE-NUCLEON RATES

Neutrino and antineutrino capture rates on free nucleons,

$$\nu_e + n \rightarrow p + e^- , \tag{34a}$$

$$\bar{\nu}_e + p \rightarrow n + e^+ , \tag{34b}$$

are important in the context of nucleosynthesis in supernovae (Qian et al. 1993). Assuming a Fermi-Dirac zero chemical potential neutrino distribution, the expression for the free nucleon neutrino or antineutrino capture rate is

$$\lambda_{\nu(\bar{\nu})} = \frac{\ln 2}{\langle ft \rangle} \Gamma \int_{E_{TH}/T_\nu}^{\infty} \left(\frac{Q_n}{kT_\nu} + x\right)^2 x^2 (e^x + 1)^{-1} dx . \tag{35}$$

Here $T_\nu(T_{\bar\nu})$ refers to neutrino (antineutrino) temperature as appropriate. The effective ft-value (from FFN II) is $\log_{10}(ft) \approx 3.035$ for both transitions in equations (34a) and (34b). Note that recent cryogenic measurements of the neutron decay lifetime (cf. Mampé et al. 1989) provide a more accurate value of the axial vector coupling constant, which in turn implies $\log_{10}(ft) \approx 3.046$ (Gould 1995) for the free nucleons. For neutrino capture on neutrons $Q_n \approx 1.293$ MeV, and $Q_n \approx -1.293$ MeV for antineutrino capture on protons. There is no threshold for neutrino capture on neutrons. However, for antineutrino capture on protons, there is a threshold of ≈ 1.8 MeV. The difference in threshold energy for the two reactions can cause a sizable difference between neutrino and antineutrino capture rates. For example, if the luminosities are equal at $L_\nu \approx L_{\bar\nu} \approx 3.5 \times 10^{51}$ ergs and the temperatures are equal, $T_\nu \approx T_{\bar\nu} \approx 4$ MeV, then the rates are $\lambda_{\nu n} \approx 3.09\ s^{-1}$ and $\lambda_{\bar\nu p} \approx 2.31\ s^{-1}$ at a radius of 10^7 cm. Although the neutrino and antineutrino temperatures are taken as equal in this example, the capture rates differ considerably.

In the regime where all nucleons are free, the electron fraction Y_e is determined by the neutrino and antineutrino capture rates (Qian et al. 1993). When all of the baryons are in free nucleons, and for the above conditions on the neutrino spectra, the resulting equilibrium electron fraction is $Y_e \approx 0.57$. The material is proton-rich, despite the equality of the temperatures of the neutrino species. This is due to the difference in Q-value between the two reactions. If the temperatures are different, while the luminosities remain the same (e.g., $T_\nu = 3.8$ MeV and $T_{\bar\nu} = 4.8$ MeV), then the equilibrium value of the electron fraction is $Y_e \approx 0.51$. The material is still proton rich, despite a significant difference in the temperatures. If the luminosities are not quite equal, for example $L_\nu \approx 12.56 \times 10^{51}$ ergs s^{-1} and $L_{\bar\nu} \approx 14.11 \times 10^{51}$ ergs s^{-1}, then the equilibrium electron fraction is $Y_e \approx 0.48$. In this case, the material is neutron rich. The electron fraction is very sensitive to the luminosities of the distribution as well as to the temperatures.

Because small changes in the variables involved in antineutrino and neutrino capture cause large changes in Y_e, we recommend using the actual neutrino spectrum (e.g., from a detailed calculation such as that of R. Mayle and J. Wilson as employed in Woosley et al. 1994) instead of a fit to the Fermi-Dirac distribution when calculating the free-nucleon capture rates. Using the detailed neutrino distribution together with the cross sections for the processes in equations (34a) and (34b), we can estimate the capture rates on free nucleons with the expression

$$\lambda \approx \sum_i \sigma(E_i) f(E_i) . \tag{36}$$

Here $f(E_i)$ is the number flux of neutrinos (antineutrinos) at energy E_i. The cross section at energy E_i is given by

$$\sigma(E_i) \approx 9.54 \times 10^{-44}\ \text{cm}^2\ \langle G \rangle (E_i - Q_n)^2 , \tag{37}$$

where $\langle G \rangle$ is the average Coulomb correction factor (Fuller & Meyer 1995). In this work, for illustrative purposes, we have assumed the final-state leptons in these processes are extremely relativistic and have set $\langle G \rangle \approx 1$.

11. CONCLUSION

We have presented expressions for the calculation of neutrino and antineutrino capture rates on heavy nuclei. We have provided tables of rates for a few key nuclei and a FORTRAN code for the calculation of these rates is available on request. In addition, we have examined several issues involved in the calculation of these rates. These include the Coulomb wave correction factor, electron blocking, the effects of various distributions of Gamow-Teller strength on the capture rates, and forbidden transitions.

We have determined that the Coulomb wave correction factor for neutrino capture is approximately 1.5 in the post–core-bounce supernova environment, while for antineutrino capture it is about 0.4. We also have determined that in this environment, the effects of electron blocking and reasonable variations in the distribution of Gamow-Teller strength on the capture rates are small. We have given a treatment of neutrino and antineutrino captures rates for mirror nuclei and $N = Z$ nuclei. In addition, the rate contribution of individual discrete-state transitions was found to be small relative to the rate contributions of the resonance transitions. However, we have pointed out that considerable acceleration of the rates may occur if there is significant low-lying first-forbidden strength. This issue bears further investigation, as it may be important in supernova nucleosynthesis considerations.

We also discussed the relative magnitude of antineutrino and neutrino capture on a single nucleus in terms of the numbers of neutrons and protons and the binding energy of the nucleus. We have found that these competing rates are comparable for nuclei near, but on the neutron-rich side of, the most tightly bound nuclear species in an A-chain.

These rates for neutrino and antineutrino capture on heavy nuclei may be used in calculations of nucleosynthesis in post–core-bounce supernovae. The effect of these rates on the final nucleosynthesis can only be judged by their inclusion in the calculations.

We would like to acknowledge useful conversations with R. Hoffman, B. Meyer, Y.-Z. Qian, P. Vogel, and S. E. Woosley. We would also like to acknowledge the helpful commments of R. Gallino. This work was supported by NSF grant PHY95-03384 and an IGPP-LLNL minigrant at UCSD.

REFERENCES

Bertsch, G. F., & Esbensen, H. 1987, Rep. Prog. Phys., 50, 607
Browne, E., Dairiki, J. M., Doebler, R. E., Shihab-Eldin, A. A., Jardine, L. J., Tuli, J. K., & Buyrn, A. B. 1978, Table of Isotopes, ed. C. M. Lederer & V. S. Shirley (New York: Wiley)
Domogatsky, G. V., & Nadyozhin, D. K. 1977, MNRAS, 178, 33P
Fuller, G. M. 1982, ApJ, 252, 741
Fuller, G. M., Fowler, W. A., & Newman, M. J. 1980, ApJS, 42, 447 (FFN I)
———. 1982, ApJ, 252, 715 (FFN II)
Fuller, G. M., & Meyer, B. S. 1995, ApJ, 453, 792
Gaarde, C., et al. 1981, Nucl. Phys. A, 369, 258
Gould, R. J. 1995, private communication
Hoffman, R. D., Woosley, S. E., Fuller, G. M., & Meyer, B. S. 1995, ApJ, submitted
Mampé, W., et al. 1989, Phys. Rev. Lett., 63, 593
Meyer, B. S., Mathews, G. J., Howard, W. M., Woosley, S. E., & Hoffman, R. 1992, ApJ, 399, 656
Qian, Y.-Z., Fuller, G. M., Mathews, G. J., Mayle, R. W., Wilson, J. R., & Woosley, S. E. 1993, Phys. Rev. Lett., 71, 1965
Seeger, P. A., & Howard, W. M. 1975, Nucl. Phys. A, 238, 491
Woosley, S. E., & Hoffman, R. 1992, ApJ, 395, 202
Woosley, S. E., Mathews, G. J., Wilson, J. R., Hoffman, R. D., & Meyer, B. S. 1994, ApJ, 433, 229
Zyranova, L. N. 1963, Once-Forbidden Beta-Transitions (New York: Macmillan)